IJBEM
Vol. 7, No. 2, 2005

Line-source Modeling and Estimation with Electroencephalography

Nannan Cao[1], İmam Şamil Yetik[1], Arye Nehorai[1], Carlos H. Muravchik[2], and Jens Haueisen[3]
[1] Department of Electrical and Computer Engineering, University of Illinois at Chicago, IL, USA
[2]Departamento de Electrotecnia, Facultad de Ingeniería, Universidad Nacional de La Plata, Argentina
[3]Neurological University Hospital, Philosophenweg 3D-07740 Jena, Germany

***Abstract*— We develop three parametric models for electroencephalography (EEG) to estimate current sources that are spatially distributed on a line. We assume a realistic head model and solve the EEG forward problem using the boundary element method. We present the models with increasing degrees of freedom, provide the forward solutions, and derive the maximum likelihood estimates as well as Cramér-Rao bounds of the unknown source parameters. A series of experiments are conducted to evaluate the applicability of the proposed models. We use numerical data to demonstrate the usefulness of our line-source models in estimating extended sources. We also apply our models to the real EEG data of N20 response that is known to have an extended source. We observe that the line-source models explain the N20 measurements better than the dipole model.**

***Keywords* — EEG, extended source modeling, Cramér-Rao bounds**

I. Introduction

Electroencephalography (EEG) is a non-invasive technique to analyze the spatial and temporal activities in the brain. It has a high temporal resolution on the order of a few milliseconds and can be used in clinical applications [1] as well as neuroscience [2]. The EEG inverse problem consists of inferring the locations and signals of the underlying neural activities from the electric potentials measured on the scalp with a sensor cap. It is ill-posed, and prior constraints need to be applied to obtain a unique solution [3].

Choosing an appropriate source model is an important step in solving the inverse problem. Most often, it is assumed that the source is small compared with its distances to the sensors and thus a current dipole is used to model it [4], [5]. Clearly, this approach is valid only if the electric activity is confined to a very small area. Multiple dipoles might be useful for modeling more separated and individually concentrated sources, where it is critical to obtain a correct estimate of the number of sources, and the estimation performance will degrade if the electric activities are spread over a large area [3]. Distributed source models reconstruct the brain activities on a 3-D grid where each point is considered as a possible location of a current dipole source, therefore the restriction on the number of dipoles can be removed [3], [6]. However, this approach is highly underdetermined and has a high computational cost. The ill-posed problem can be tackled by using regularization techniques [7] and iterative focalization approaches [8], but these methods still have high computational load for sophisticated source models [6].

This work was supported by the National Science Foundation Grant CCR-0105334.

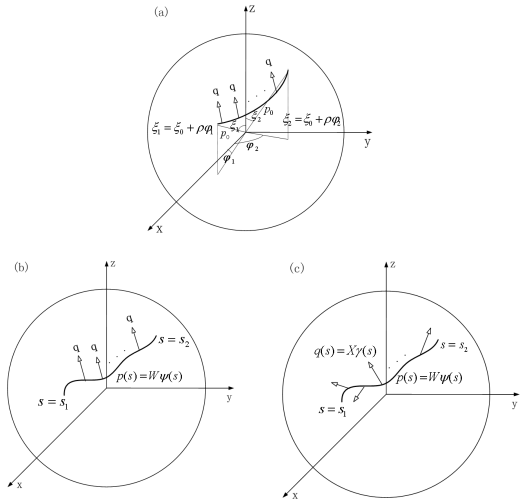

Fig. 1. Illustration of the three line-source models. (a) CRCM model, (b) VPCM model, (c) VPVM model. See Section II for more details.

In this paper, we present three parametric line-source models for EEG assuming a realistic head model, extending our previous work on magnetoencephalography (MEG) source modeling [9]. In Section II, we describe the line-source models and the corresponding EEG forward models in a kernel-matrix form. In Section III, we derive the maximum likelihood estimates (MLEs) and the Cramér-Rao bounds (CRBs) of the unknown parameters. We give numerical examples in Section IV and conclude this paper in Section V.

II. Source and Measurement Models

We present below three parametric line-source models with increasing degrees of freedom and provide the EEG forward models in a uniform kernel-matrix form.

A. Line-source Models

Constant-radius Constant-moment (CRCM) Model: In this model, the source position is an arc with an arbitrary orientation on a spherical surface: it has a fixed distance from the head center, its azimuth varies within a certain interval, and

its elevation changes linearly with the azimuth. The source moment is assumed to be uniformly distributed along the arc; see Fig. 1a. Using spherical coordinates with p representing the distance from the center, ξ the elevation, and φ the azimuth, we have

$$\begin{aligned} \boldsymbol{J}(\boldsymbol{r},t) &= \boldsymbol{q}(t)\delta(p-p_0)\delta(\xi-\xi_0-\rho\varphi) \\ &\quad \times[u(\varphi-\varphi_1)-u(\varphi-\varphi_2)], \qquad (1) \\ \boldsymbol{q}(t) &= [q_x(t),q_y(t),q_z(t)]^T, \qquad (2) \end{aligned}$$

where p_0 is the fixed radius, φ_1 and φ_2 the azimuth limits, and ξ_0 the constant elevation. The slope ρ determines the source orientation, and $u(\varphi)$ is the unit step function defined as $u(\varphi) = 1$ for $\varphi > 0$ and $u(\varphi) = 0$ for $\varphi \leq 0$. Thus, in this model the unknown position parameter vector is $\boldsymbol{\theta}_{\rm p} = [p_0, \xi_0, \rho, \varphi_1, \varphi_2]^T$.

Variable-position Constant-moment (VPCM) Model: This model provides more degrees of freedom for the source position than the CRCM model: the source position is allowed to be a parametric curve in 3-D space instead of an arc on a spherical surface; see Fig. 1b. We represent the source position in Cartesian coordinates as

$$\boldsymbol{p}(s) = [p_x(s), p_y(s), p_z(s)]^T, \qquad s \in [s_1, s_2], \qquad (3)$$

where s is the curve parameter with limits s_1 and s_2. Accordingly, the source current density becomes

$$\begin{aligned} \boldsymbol{J}(\boldsymbol{r},t) &= \\ &\begin{cases} \boldsymbol{q}(t) & \boldsymbol{r} = [p_x(s), p_y(s), p_z(s)]^T, s \in (s_1, s_2), \\ 0 & \text{elsewhere}, \end{cases} \qquad (4) \\ \boldsymbol{q}(t) &= [q_x(t), q_y(t), q_z(t)]^T. \qquad (5) \end{aligned}$$

Variable-position Variable-moment (VPVM) Model: This is the most general model: the source position consists of a parametric curve and the source moment is allowed to vary along the position; see Fig. 1c. Hence, the current density is

$$\begin{aligned} \boldsymbol{J}(\boldsymbol{r},t) &= \\ &\begin{cases} \boldsymbol{q}(s,t) & \boldsymbol{r} = [p_x(s)\ p_y(s)\ p_z(s)]^T, s \in (s_1, s_2), \\ 0 & \text{elsewhere}, \end{cases} \qquad (6) \\ \boldsymbol{q}(s,t) &= [q_x(s,t), q_y(s,t), q_z(s,t)]^T. \qquad (7) \end{aligned}$$

B. Measurement Model

We use the boundary element method [5], [10] to solve the EEG forward problem for a realistic head model. We pose the quasi-static Maxwell's equations as 2-D integrals on all inter-layer surfaces in the head and tessellate each surface into small triangular elements. We approximate the electric potentials by a linear combination of basis functions and solve the boundary integrals using the weighted residual technique. We have shown in [11] that for each source model, considering K independent trials and $N_{\rm t}$ time samples, the measured potentials at time t in the kth trial can be written as:

$$\boldsymbol{y}_k(t) = A(\boldsymbol{\theta}_{\rm p})\boldsymbol{m}(t) + \boldsymbol{e}_k(t), \quad t = 1,\ldots,N_{\rm t},\ k = 1,\ldots,K, \qquad (8)$$

where the vector $\boldsymbol{\theta}_{\rm p}$ represents the source location parameters, $\boldsymbol{m}(t)$ the moment parameters, $\boldsymbol{y}_k(t)$ the measurements, $A(\boldsymbol{\theta}_{\rm p})$ the array response matrix, and $\boldsymbol{e}_k(t)$ the additive noise.

The terms $A(\boldsymbol{\theta}_{\rm p})$, $\boldsymbol{\theta}_{\rm p}$, and $\boldsymbol{m}(t)$ assume different expressions for different line-source models; see [11] for more details. Furthermore, $A(\boldsymbol{\theta}_{\rm p})$ is always in the form of

$$A(\boldsymbol{\theta}_{\rm p}) = H_{\rm E}(D+H)^{\dagger}V(\boldsymbol{\theta}_{\rm p}), \qquad (9)$$

where "†" represents the pseudoinverse. Each entry of matrices $H_{\rm E}$, D and H is a surface integral on a certain tessellation element, depending only on the EEG sensor configuration and the head geometry. Therefore, source parameters only appear in V, which is desirable for reducing the computational cost.

III. Maximum Likelihood Estimates and Cramér-Rao Bounds

We use the maximum likelihood method to estimate the source parameters $\boldsymbol{\theta}_{\rm p}$ and $\boldsymbol{m}(t)$. Assuming zero-mean Gaussian noise that is spatially and temporarily uncorrelated, the MLE of $\boldsymbol{\theta}_{\rm p}$ is [4], [9]

$$\hat{\boldsymbol{\theta}}_{\rm p} = \arg\min_{\boldsymbol{\theta}_{\rm p}} \sum_{t=1}^{N_{\rm t}} -\bar{\boldsymbol{y}}(t)^T P(\boldsymbol{\theta}_{\rm p})\bar{\boldsymbol{y}}(t), \qquad (10)$$

where

$$\begin{aligned} \bar{\boldsymbol{y}}(t) &= 1/K \sum_{k=1}^{K} \boldsymbol{y}_k(t), \qquad (11) \\ P(\boldsymbol{\theta}_{\rm p}) &= A(\boldsymbol{\theta}_{\rm p})[A(\boldsymbol{\theta}_{\rm p})^T A(\boldsymbol{\theta}_{\rm p})]^{-1} A(\boldsymbol{\theta}_{\rm p})^T. \qquad (12) \end{aligned}$$

The MLE of $\boldsymbol{m}(t)$ is

$$\hat{\boldsymbol{m}}(t) = [A(\hat{\boldsymbol{\theta}}_{\rm p})^T A(\hat{\boldsymbol{\theta}}_{\rm p})]^{-1} A(\hat{\boldsymbol{\theta}}_{\rm p})^T \bar{\boldsymbol{y}}(t). \qquad (13)$$

The Cramér-Rao bound is a lower bound on the covariance of any unbiased estimator. It is independent of the algorithm used for the estimation and thus establishes a universal performance limit [12]. Let $\boldsymbol{\theta} = [\boldsymbol{\theta}_{\rm p}^T, \boldsymbol{m}(1)^T, \ldots, \boldsymbol{m}(N_{\rm t})^T]^T$ represent all the unknown source parameters, $\hat{\boldsymbol{\theta}}$ be an unbiased estimator of $\boldsymbol{\theta}$, and $\mathcal{I}(\boldsymbol{\theta})$ denote the Fisher information matrix (FIM). The Cramér-Rao inequality establishes that

$$\mathrm{E}\{(\boldsymbol{\theta}-\hat{\boldsymbol{\theta}})(\boldsymbol{\theta}-\hat{\boldsymbol{\theta}})^T\} \geq \mathrm{CRB}(\boldsymbol{\theta}) = \mathcal{I}^{-1}(\boldsymbol{\theta}). \qquad (14)$$

For the measurement model (8), assuming zero-mean Gaussian noise with covariance matrix $\Sigma = \sigma_{\rm E}^2 I_{m_{\rm E}}$, the Fisher information matrix is

$$\begin{aligned} \mathcal{I}(\boldsymbol{\theta}) &= \begin{bmatrix} \mathcal{I}_{\rm pp} & \mathcal{I}_{\rm qp}^T \\ \mathcal{I}_{\rm qp} & \mathcal{I}_{\rm qq} \end{bmatrix} \qquad (15) \\ &= \frac{K}{\sigma_{\rm E}^2} \begin{bmatrix} \mathcal{I}_{\rm pp} & \mathcal{I}_{\rm qp}^T(1) & \cdots & \mathcal{I}_{\rm qp}^T(N_{\rm t}) \\ \mathcal{I}_{\rm qp}(1) & \mathcal{I}_{\rm qq} & \cdots & 0 \\ & & \vdots & \\ \mathcal{I}_{\rm qp}(N_{\rm t}) & 0 & \cdots & \mathcal{I}_{\rm qq} \end{bmatrix}, \qquad (16) \end{aligned}$$

where

$$\mathcal{I}_{\rm pp} = \sum_{t=1}^{N_{\rm t}} D_A^T(\boldsymbol{\theta}_{\rm p})[(\boldsymbol{m}(t)\boldsymbol{m}^T(t)) \otimes I_{m_{\rm E}}]D_A(\boldsymbol{\theta}_{\rm p}), \quad (17)$$

$$\mathcal{I}_{\rm qp}(t) = A^T(\boldsymbol{\theta}_{\rm p})(\boldsymbol{m}^T(t) \otimes I_{m_{\rm E}})D_A(\boldsymbol{\theta}_{\rm p}), \quad (18)$$

$$\mathcal{I}_{\rm qq} = A^T(\boldsymbol{\theta}_{\rm p})A(\boldsymbol{\theta}_{\rm p}), \quad (19)$$

$I_{m_{\rm E}}$ is an $m_{\rm E} \times m_{\rm E}$ identity matrix, "$\otimes$" denotes the Kronecker product [14], and $D_A(\boldsymbol{\theta}_{\rm p})$ is defined as [4], [9]

$$D_A(\boldsymbol{\theta}_{\rm p}) \triangleq \frac{\partial \text{vec}(A(\boldsymbol{\theta}_{\rm p}))}{\partial \boldsymbol{\theta}_{\rm p}^T}. \quad (20)$$

Utilizing the structure of $A(\boldsymbol{\theta}_{\rm p})$ in (9), we rewrite $D_A(\boldsymbol{\theta}_{\rm p})$ as

$$D_A(\boldsymbol{\theta}_{\rm p}) = \frac{\partial \text{vec}(A(\boldsymbol{\theta}_{\rm p}))}{\partial \boldsymbol{\theta}_{\rm p}^T} \quad (21)$$

$$= (I_{n_{\rm p}} \otimes (H_{\rm E}(D+H)^{\dagger})) \cdot \frac{\partial \text{vec}(V(\boldsymbol{\theta}_{\rm p}))}{\partial \boldsymbol{\theta}_{\rm p}^T}, \quad (22)$$

where $n_{\rm p}$ is the number of unknown position parameters and $I_{n_{\rm p}}$ is an $n_{\rm p} \times n_{\rm p}$ identity matrix. In this way, we need to calculate only the second part of (22) for any possible $\boldsymbol{\theta}_{\rm p}$, reducing the computational cost to obtain CRBs for a certain subject.

IV. Numerical Examples

We conducted a series of experiments to demonstrate the applicability of the proposed models in estimating the line sources. We used a three-layer realistic head model composed of the brain, skull, and scalp, and assumed the conductivity values to be $0.33\Omega^{-1}\text{m}^{-1}$ for the scalp and brain, and $0.0042\Omega^{-1}\text{m}^{-1}$ for the skull [10]. The inter-layer surfaces were tessellated into a total of 9290 triangles (2884 on the brain, 3240 on the skull, and 3166 on the scalp) through MRI (Philips, Hamburg, Germany). We used an EEG cap consisting of 32 electrodes (Philips, Hamburg, Germany), whose positions are adjusted for each subject. For the BEM, we used linear discretization [5] and chose the weighting function in a collocation form.

A. Results Using Numerical EEG Data

We compared the performances of different source models and calculated the CRBs for the CRCM model. Throughout the experiments in this subsection, we selected the noise variance to obtain a signal-to-noise ratio (SNR) of 20dB. We define SNR as $\text{SNR} = 10\log((\sum_{i=1}^{m_{\rm E}} s_i^2)/\sigma_{\rm E}^2)$, where $s_i^2 = \frac{1}{N_{\rm t}}\sum_{t=1}^{N_{\rm t}} v_{{\rm E}i}^2(t)$ is the signal power at the ith sensor.

1) Comparison of different models: We assumed a source that lies along a straight line between $[x,y,z] = [12,15,60]$mm and $[x,y,z] = [40,40,52]$mm. It has a length of 38mm and a larger change in the elevation than the azimuth. We chose the moment density $\boldsymbol{q}(s) = [\boldsymbol{q}_x(s), \boldsymbol{q}_y(s), \boldsymbol{q}_z(s)]$ with $q_x = -s^2 + 400$nA, $q_y = 200$nA, and $q_z = -s^2 + 2s + 300$nA, so that it is small at the ends and large at the center. We applied the VPVM model to generate the EEG data and estimated the source parameters using all the proposed line-source models as well as the dipole source model.

TABLE I
Comparison of estimation performance using simulated data. The source is assumed to lie on a straight line between $[12,15,60]$mm and $[40,40,52]$mm. The source moment density is chosen to be $q_x = -s^2 + 400$nA, $q_y = 200$nA, and $q_z = -s^2 + 2s + 300$nA, where s is the curve parameter.

Source model	No. of para.	MSE(μV^2)	AIC
Dipole	6	1.65	108.77
CRCM	8	1.32	103.16
VPCM	9	0.91	96.27
VPVM	15	0.63	101.29

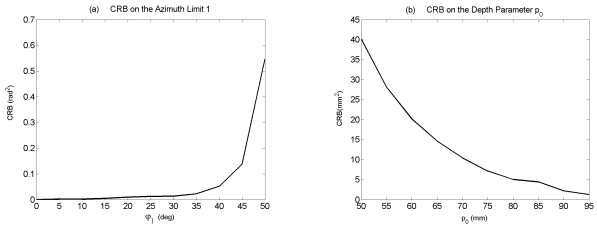

Fig. 2. The Cramér-Rao bounds on the unknown source position parameters for the CRCM model (SNR=20dB). (a) $p_0 = 85$mm, $\xi_0 = 45^\circ$, $\rho = 0$, and $\varphi_2 = 60^\circ$; (b) $\xi_0 = 45^\circ$, $\rho = 0$, $\varphi_1 = 20^\circ$, and $\varphi_2 = 60^\circ$.

We analyzed the estimation accuracy and model fitness using the mean-squared error (MSE) and the Akaike's information criterion (AIC) [15]. The AIC penalizes the log-likelihood function for additional source parameters, and hence accounts for the trade-off between model complexity and accuracy. For normally distributed noise with variance σ^2,

$$\text{AIC} = \ln((2\pi)^{mN_tK}\sigma^2) + \frac{\sum_{t=1}^{N_{\rm t}}\sum_{j=1}^{K} \boldsymbol{e}_j^T(t)\boldsymbol{e}_j(t)}{\sigma^2} + 2g, \quad (23)$$

where g is the number of unknown parameters, and $\boldsymbol{e}_j(t)$ is the noise at the tth time sample in the jth trial. Hence, a smaller AIC value indicates a better fit of the model.

The simulation results are shown in Table I. We observe that the line-source models have smaller MSEs and AICs than the dipole model, showing that line-source models can explain the data better than the focal one if the real source is extended sufficiently.

2) Cramér-Rao bound results: We computed the CRBs for the CRCM model, and analyzed the bounds on the variance of the position parameters in order to investigate the effects of the source length and depth on the estimation performance. We chose a moment density $\boldsymbol{q} = [100,100,100]^T$nA and set $\rho = 0$. The CRB results are shown in Fig. 2. Fig. 2a is the CRB for φ_1 with $p_0 = 85$mm, $\xi_0 = 45^\circ$, and $\varphi_2 = 60^\circ$; and Fig. 2b for p_0 with $\xi_0 = 45^\circ$, $\varphi_1 = 20^\circ$, and $\varphi_2 = 60^\circ$.

We observed from the CRB values that

- Longer sources result in smaller CRB on the azimuth limit; that is, it is easier to estimate longer sources. Fig. 2a shows that we can estimate φ_1 with standard deviation less than 3° for a source longer than 12mm, at a depth of $p_0 = 85$mm and elevation $\xi = 45^\circ$.

TABLE II

ESTIMATION PERFORMANCE RESULTS FOR REAL EEG MEASUREMENTS OF N20 RESPONSES.

Subject	A	B	C	D
MSE (dipole) (μV^2)	3.54	1.26	2.69	1.98
MSE (VPVM)(μV^2)	2.76	1.04	2.20	1.35
Error decreased (%)	22	17	18	31
Est. source length (cm)	2.34	1.89	2.56	2.14

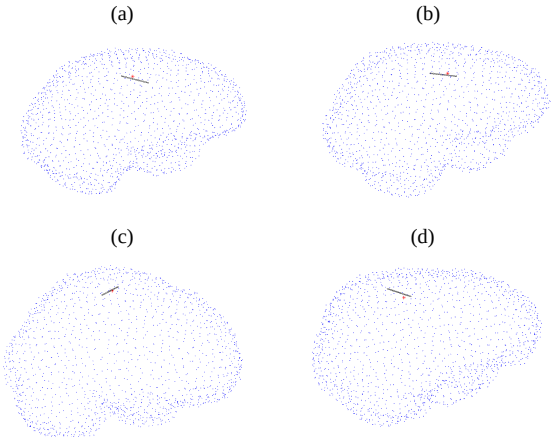

Fig. 3. Estimated line and dipole sources for real EEG measurements of N20 responses (in the brain mesh).

- Deeper sources produce larger CRBs of the depth component p_0. We can infer from Fig. 2b that the source depth can be estimated with less than 3mm error if the source is more than 70mm away from the head center. Therefore, deeper sources result in worse estimation accuracy.

B. Results Using Real EEG Data

We now present results using real EEG measurements of N20 response from four healthy human subjects. The data were recorded over the contralateral somatosensory cortex when square-wave current pulses of 0.2ms were delivered to the right or left wrist at a stimulation rate of 4Hz. The data were sampled at 5000Hz with a 1500Hz anti-aliasing low-pass filter, resulting in 250 time samples for each subject.

We applied the VPVM model and the dipole model to estimate the source parameters. We computed the MSEs and also estimated the source length. We can see from the Table II that the VPVM model has a smaller MSE than the dipole model. In Fig. 3, we plotted the estimated dipole source and line source for each subject in the brain meshes obtained from MRI.

V. CONCLUSION

We proposed three parametric line-source models for EEG with increasing degrees of freedom. We assumed a realistic head model and solved the EEG forward problem using the boundary element method. We derived the MLEs and CRBs of the source parameters and evaluated the model fitness using the MSE and AIC values. The main results can be summarized as follows:

- Numerical results showed that the proposed line-source models perform better than the dipole source model for extended sources.
- The CRB of the position parameters indicated that longer sources result in better estimation accuracy, and deeper sources produce poorer performance.
- The proposed models explained the real EEG measurements of N20 responses better than the dipole source model.

Among the possible extensions of the present work is the surface-source modeling for EEG. It is useful especially for the epileptic sources that are usually extended over a large area. With enough prior information, we may improve the modeling precision and estimation performance by choosing basis functions (see details in [11]) according to the tissue shape information obtained from MRI instead of using polynomials. Furthermore, we can also incorporate more complex noise models (e.g., unknown spatially correlated noise) and obtain the MLEs of the unknown parameters using the extended GMANOVA technique as in [4].

REFERENCES

[1] W. W. Orrison, Jr., J. D. Lewine, J. A. Sanders, and M. F. Hartshorne, *Functional Brain Imaging*. St. Louis, MO: Mosby-Year Book, 1995.

[2] E. Niedermeyer and F. L. Silva, *Electroencephalography. Basic Principles, Clinical Applications and Related Fields*. Urban and Schwarzenberg Inc., Baltimore, 1987.

[3] C. M. Michel, M. M. Murray, G. Lantz, S. Gonzalez, L. Spinelli, and R. G. de Peralta, "EEG source imaging," *Clin. Neurophysiol.*, vol. 115, pp. 2195-2222, 2004.

[4] A. Dogandzic and A. Nehorai, "Estimating evoked dipole responses in unknown spatially correlated noise with EEG/MEG arrays," *IEEE Trans. Signal Process.*, Vol. SP-48, pp. 13-25, 2000.

[5] J. C. Mosher, R. M. Leahy, and P. S. Lewis, "EEG and MEG: Forward solutions for inverse methods," *IEEE Trans. Biomed. Eng.*, vol. 46, pp. 245-259, 1999.

[6] L. Gavit, S. Baillet, J. Mangin, J. Pescatore, and L. Garnero, "A multiresolution framework to MEG/EEG source imaging," *IEEE Trans. Biomed. Eng.*, vol. 48, pp. 1080-1087, 2001.

[7] R. Pascula-Marqui *et al.*, "Low resolution electromagnetic tomography: A new method for localizing electrical activity of the brain," *Int. J. Phychophysiol.*, vol. 18, pp. 49-65, 1994.

[8] I. Gorodnistky, J. George, and B. Rao, "Neuromagnetic imaging with FOCUSS: A recursive weighted minimum-norm algorithm," *Electroencephalogr. Clin. Neurophysiol.*, vol. 95, pp. 231-251, 1995.

[9] I. S. Yetik, A. Nehorai, C. Muravchik, and J. Haueisen, "Line-source modeling and estimation with magnetoencephalography," to appear in *IEEE Trans. Biomed. Eng.*, vol. 52, 2005.

[10] C. Muravchik and A. Nehorai, "EEG/MEG error bounds for a static dipole source with a realistic head model," *IEEE Trans. Signal Process.*, Vol. SP-49, pp. 470-484, 2001.

[11] Nannan Cao, İmam Şamil Yetik, Arye Nehorai, Carlos H. Muravchik, and Jens Haueisen, "Line-source modeling and estimation for electroencephalography," *unpublished*.

[12] S. M. Kay, *Fundamentals of Statistical Signal Processing: Estimation Theory*. PTR Prentice Hall, New Jersey, 1993.

[13] J. C. Mosher, R. M. Leahy, and P. S. Lewis, "Matrix kernels for MEG and EEG source localization and imaging," *Acoust., Speech, Signal Processing, IEEE Intl. Conf.*, vol. 5, 1995, pp. 2943 - 2946.

[14] J. W. Brewer, "Kronecker products and matrix calculus in system theory," *IEEE Trans. Circuits and Syst.*, vol. 25, pp. 772-781, 1978.

[15] H. Akaike, "Information and an extension of the likelihood principle," *Proc. Int. Symp. on Information Theory*, Supplement to Problems of Control and Information Theory, Budapest, 1973, pp. 267-281.